Friction **11**(7): 1349–1358 (2023)
https://doi.org/10.1007/s40544-022-0688-4
ISSN 2223-7690
CN 10-1237/TH
RESEARCH ARTICLE

Fingerprint-inspired surface texture for the enhanced tip pinch performance of a soft robotic hand in lubricated conditions

Tianze HAO†, Huaping XIAO*,†, Shuhai LIU*, Yibo LIU
College of Mechanical and Transportation Engineering, China University of Petroleum-Beijing, Beijing 102249, China
Received: 04 June 2022 / Revised: 21 July 2022 / Accepted: 26 August 2022

Abstract: The core capabilities of soft grippers/soft robotic hands are grasping and manipulation. At present, most related research often improves the grasping and manipulation performance by structural design. When soft grippers rely on compressive force and friction to achieve grasping, the influence of the surface microstructure is also significant. Three types of fingerprint-inspired textures with relatively regular patterns were prepared on a silicone rubber surface via mold casting by imitating the three basic shapes of fingerprint patterns (i.e., whorls, loops, and arches). Tribological experiments and tip pinch tests were performed using fingerprint-like silicone rubber films rubbing against glass in dry and lubricated conditions to examine their performance. In addition to the textured surface, a smooth silicone rubber surface was used as a control. The results indicated that the coefficient of friction (COF) of the smooth surface was much higher than that of films with fingerprint-like textures in dry and water-lubricated conditions. The surface with fingerprint-inspired textures achieved a higher COF in oil-lubricated conditions. Adding the fingerprint-like films to the soft robotic fingers improved the tip pinch gripping performance of the soft robotic hand in lubricated conditions. This study demonstrated that the surface texture design provided an effective method for regulating the grasping capability of humanoid robotic hands.

Keywords: fingerprint-like patterns; surface engineering; soft hand; tip pinch

1 Introduction

Grasping is defined as the ability to pick up and hold an object despite external interference, while manipulation is the ability to apply a force to an object to rotate and displace it relative to the reference frame of the manipulator [1]. These features represent the core capabilities of soft grippers/soft robotic hands. The current research often focuses on the structural design to improve the grasping and manipulation ability. There are mainly three categories of grippers inspired by nature: muscular hydrostats, spinal grippers, and manual grippers [2]. The muscular hydrostats inspired by octopus arms typically have infinite degrees of freedom and rely on a soft body to passively adapt to the shape and size of the grasped object [3–5], while the suction cups designed on the surface enhance the grasping ability [6]. Similarly, the skeletal joints in spinal grippers are shorter towards the tips, and the geometric shape can be effectively adapted to the objects [7, 8]. Anthropomorphic grippers are also an excellent choice for grasping. Since human hands need to be compatible with the everyday environment, the design and development of soft robotic hands range from two-fingered and three-fingered structures to articulated fingers and palms [9–14]. In addition to mechanical interlocking, where the gripper wraps the object and uses compressive force to operate, the friction between the two surfaces helps stabilize the grasping. The surface microstructure significantly influences the friction required for grasping and manipulation, while the fingerprint-like microstructure

† Tianze HAO and Huaping XIAO contributed equally to this work.
* Corresponding authors: Huaping XIAO, E-mail: hxiao@cup.edu.cn; Shuhai LIU, E-mail: liu_shu_hai@163.com

presents unique grasping advantages. The skin of a fingerprint stretches to different degrees when grasping objects and the gully-shaped patterns enhance the grasping ability while protecting the fingers in unpredictable situations. In a wet system, fingerprints can help expand the contact area, increasing the probability of grasping success to some extent [15–18]. Wet-induced wrinkles are drainage networks for channeling away water during grip，and it is pliable so that the liquid passes through the channels between the wrinkles, and keep the entire skin of the finger in contact with the surface [19]. This differs from the adhesion effect of tree frog toes and gecko claw bristles, in which the microstructure size is at the micro-nano scale [20–22]. Human fingerprints are relatively macroscopic and mainly rely on changing the friction to improve grasping. Minimal research is currently available regarding the effect of macroscopic microstructures on the grasping ability of manipulators, especially that of fingerprint-like irregular patterns.

Whether it is a gripper or a soft hand, testing is commonly conducted in dry conditions when using compressive force and friction to achieve grasping or manipulation. The grasping performance is characterized by changing the shape, size, weight, and contact surface of the grasped object [23–26]. Contrarily, manipulator testing methods are more diverse and include actions such as kneading dough, drawing poker, and twisting bottle caps [27, 28]. In addition to dry conditions, underwater grasping is another testing method designed to explore grasping capabilities and effects in underwater environments [29]. Water- and oil-lubricated conditions commonly affect the grasping/operating effect during daily life or industrial production. Therefore, to expand the soft hand application range, it is necessary to examine its grasping performance in lubricated conditions.

Tribological tests were conducted with rigid friction pairs in dry, water-lubricated, and oil-lubricated conditions. Three types of film with relatively regular patterns were fabricated on a silicone rubber surface via fine mold casting by imitating the three basic fingerprint patterns (loops, whorls, and arches). Then, the fingerprint-like films were added to the soft robotic fingers to explore the specific differences between these films and the smooth film regarding the precise grasping action (tip pinch). Figure 1(c) shows the other components besides the operation module. The relationship between the friction structure and complicated textural patterns of the highly complex three-dimensional (3D) fingerprint-like surface was analyzed by combining the principles of contact mechanics and tribology.

2 Materials and methods

2.1 Materials

According to Young's modulus of human soft tissue and skin [30], Mold star 30 (hardness = 30 A, Smooth-On Ltd.), was used to fabricate the soft, fingerprint-like films and was the same material used for creating the soft robotic hand in our previous work [31]. The robotic finger was manufactured using Eco-Flex 00-50 (hardness = 50 D, Smooth-On Ltd.) silicone rubber. The mechanical properties of two materials were measured using a single-arm uniaxial stretcher (LN-0939CS, Guangdong LiNa Industrial), with the spindle tensile specimens shown in Fig. S1 in the Electronic Supplementary Material (ESM). The stress–strain curves of the Mold star 30 and Eco-Flex 00-50 silicone materials are shown in Fig. S2 in the ESM.

2.2 Preparation of the soft films with fingerprint-like textures

Human fingerprints usually display complex irregular patterns, divided into three categories according to the tendency of the fingerprint peaks: loops, whorls, and arches. The silicone rubber films were prepared via fine mold casting by imitating the heights between the fingerprint peaks and valleys and the distances between the fingerprint peaks. Molds with different patterns (loops, whorls, and arches) were printed using a PolyJet 3D printer (J750, Stratasys) and photosensitive resin (VeroWhite FullCure 835). Two silicone rubber liquid components were mixed until completely homogeneous and placed in a vacuum box, where a rotary-vane vacuum pump (VP-1, ZhengKong) was used for degassing the bubbles. Then, a thin layer of mold release agent (Ease Release 200, Smooth-On) was applied to the molds, after which

the degassed silicone rubber was poured inside. 24 h was allowed to fully cure and remove the films. The films were then treated in an ultrasonic cleaner for 15 min to remove the residual release agent on the surface. The subsequent silicone rubber film was rectangular with a length of 25 mm, a width of 20 mm, and a thickness of about 1 mm (Fig. 1(a)). The 3D morphology of the silicone rubber films with fingerprint-like textures was characterized using a 3D optical microscope (VK-X100, KEYENCE). In addition, the silicone rubber film with a smooth surface was prepared in the same way as the fingerprint-like silicone rubber films.

2.3 Preparation of the friction test platform

This study built a unique friction testing platform mainly composed of an operation module, a pull force sensor, a signal collector, a motor controller, and a power supply. Figure 1(b) shows the various parts of the operation module. The dark blue silicone rubber film with the fingerprint-like texture was attached to a piece of light blue silicone rubber (hardness = 36 A; Smooth-Sil 936, Smooth-On). Various iron blocks were placed on top to obtain different load sizes. The motorized linear translation stage (MTS50-Z8, Thorlabs) realized linear movement in the horizontal direction under the control of the motor controller (KDC101, Thorlabs), while the motion acceleration and maximum movement speed could be adjusted as required. Figure 1(c) shows the other components besides the operation module. The real-time friction force was collected by the pull force sensor (LCM6, MTO) and the signal amplifier (FC400, Unipulse). The vertical position of the silicone rubber film was adjusted via a single-axis flexure stage (NFL5D, Thorlabs) to reach the critical state of contact with the glass plate.

2.4 Tribological test

During the tribological test, the soft film moved horizontally on the smooth rigid surface (glass plate) under a specific load to imitate the tribological phenomenon between the finger pad and the object when the soft robotic hand realized an antipodal precise grasping action. The glass plate was cleaned sequentially with absolute ethanol and deionized water. The tests were conducted by controlling a single variable. The relative displacement was fixed at 10 mm at an acceleration of 1.5 mm/s^2. The tribological tests were performed in dry conditions at different maximum relative motion speeds and loads. The maximum speed was selected according to gradients of 0.5, 1, 1.5, 2, and 2.4 mm/s. The upper limit of the speed of the motorized linear translation stage was

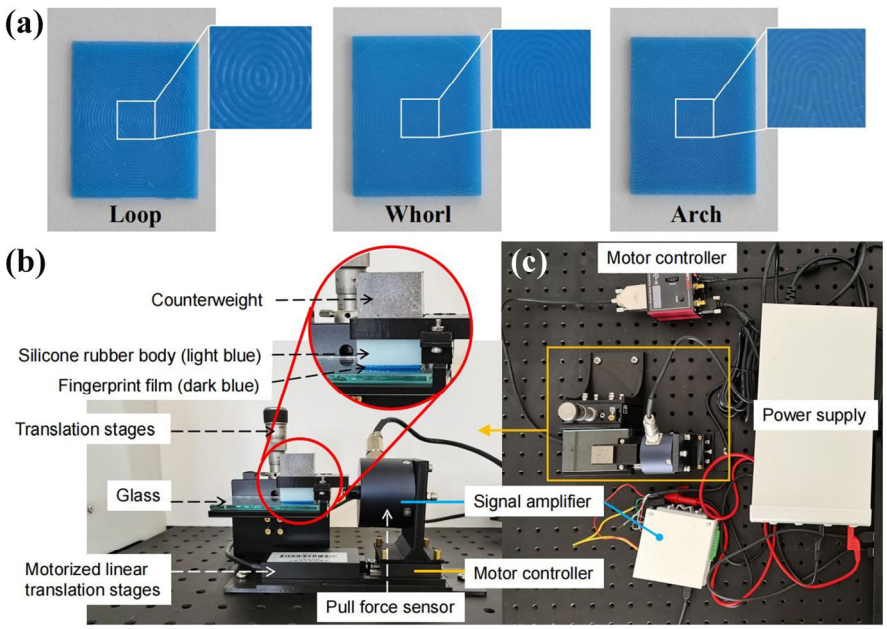

Fig. 1 (a) Silicone rubber films with fingerprint-like textures (loops, whorls, and arches). (c, d) Configuration of the friction testing platform.

2.4 mm/s. As shown in Fig. 1, the contact load was achieved by replacing the counterweight (iron block) at 2.38, 3.03, 3.79, 4.99, 7.79, 10.17, and 11.79 kPa, respectively. During the tribological test of the smooth-surfaced silicone rubber, the side in contact with the glass plate (above) flowed naturally during the pouring process, unlike the side in contact with the mold.

The tribological lubrication tests were conducted at a load of 7.79 kPa and a sliding speed of 0.5 mm/s in water-lubricated and oil-lubricated conditions. Before each experiment, full contact was facilitated between the lubrication medium and the soft friction pair to ensure complete lubrication. Each tribological test was performed in ambient conditions and was repeated at least fifteen times.

2.5 Tip pinch test using soft robotic fingers

A pneumatic soft robotic hand with a multi-jointed structure was designed in our previous work [31]. In this study, the soft hand was used as a carrier with the fingerprint-like films attached to the finger pads in the same positions as human fingerprints to achieve the tip pinch action. Tip pinch referred to an antipodal precision grasp action between the thumb tip and index fingertip [32] and was used to test the firmness of precise grasping.

As shown in Fig. S3 in the ESM, air (40 kPa) was used to stretch out the thumb and index finger of the soft hand to complete the tip pinch action. The soft hand equipped with different films was allowed to grasp two kinds of smooth objects (3D-printed boxes) with flat and curved contact surfaces. The optimal pressure for realizing grasping between the tip of the robotic finger and the object surfaces was 40 kPa. For example, sweat or sebum production or contact with water or oil may reduce grasp strength. Therefore, the grasping and manipulation ability of robotic hands may be more pronounced.

During the tip pinch tests, quartz and ceramic sand were used as counterweights (Fig. S4 in the ESM). The soft hand was allowed to clamp the smooth plastic box in dry and oil-lubricated conditions. Then, quartz sand was continuously added to the plastic box until noticeable slippage occurred, and the weight of the counterweight box was recorded. During the underwater tip pinch tests, the soft hand and the counterweight box were completely immersed in water. Since quartz sand would partially dissolve in the water, preventing an accurate weight measurement, ceramic sand was used instead. Before the tests, the ceramic sand was cleaned with water and heated in a drying oven until completely dry.

3 Results and discussion

3.1 Surface characteristics

Figures 2(a)–2(c) show the 3D morphology of the films with loop, whorl, and arch textures, respectively. The fingerprint peak heights were 300 μm, while the distances between the adjacent fingerprint peaks were about 250 μm. The red dotted lines represent the height fluctuations of the red realization position texture in the middle of the fingerprint-like film, with maximum heights of 303.038, 286.225, and 299.271 μm.

3.2 Impact of the surface texture on the COF

Figure 2(d) shows the COF of the fingerprint-like films and smooth film in dry conditions at a load of 7.79 kPa, an acceleration of 1.5 mm/s^2, and a maximum relative motion velocity ranging between 0.5–2.4 mm/s. The COF of the smooth film was significantly higher than the fingerprint-like films but decreased slowly from 2.77 to 2.45 between 0.5 and 2.4 mm/s. The COF of the films with loops, whorls, and arches gradually stabilized at a motion speed exceeding 1 mm/s, reaching about 1.25, 0.85, and 0.55, respectively.

Figures 2(e) and 2(f) show the COF and friction force of the fingerprint-like and smooth films at different contact pressures. The COF of the smooth film was significantly higher than the fingerprint-like films, exhibiting fluctuation between 2.38 and 4.99 kPa, first increasing and then decreasing. At the same contact pressure, the COF of the three fingerprint-like films gradually increased to 0.87, 0.65, and 0.45. At a contact pressure higher than 4.99 kPa, the COF decreased slightly and gradually stabilized at 0.7, 0.58, and 0.42. As shown in Fig. 2(f), the friction force increased linearly at a higher contact pressure, becoming more distinct when exceeding 4.99 kPa, which was consistent with the COF changes shown

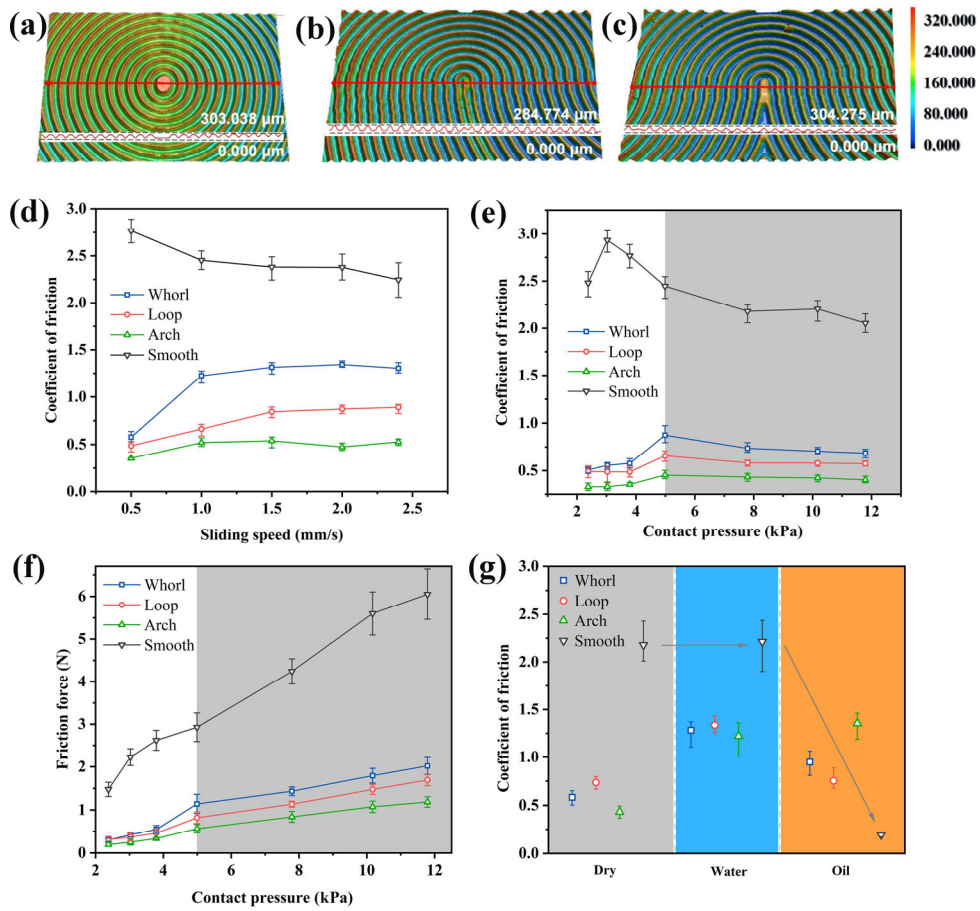

Fig. 2 (a, b, c) 3D morphologies of the films with loop, whorl, and arch textures. (d, e, g) COF values of the soft films at different sliding speeds, contact pressures, and friction conditions. (f) Friction force of the soft films at different contact pressures.

in Fig. 2(e). At a contact pressure lower than 4.99 kPa, the data was inconsistent when the load was too low due to the systematic errors of the friction testing platform. The growth rate stabilized at a higher contact pressure as the load gradually increased and exceeded the weighted sum of the soft film and light blue rubber block.

Figure 2(g) compares the COF of the silicone rubber films in dry, water-lubricated, and oil-lubricated conditions. When the fingerprint-like films were fully water-lubricated, the COF was about double that in dry conditions, reaching 1.21–1.33. In water-lubricated conditions, the COF of the smooth film displayed no significant changes, remaining at about 2.2. This was because almost no water film formation was evident between the glass plate and the smooth surface during a single friction process, rendering the COF virtually the same as dry friction conditions. In adequate oil-lubricated conditions, the COF of the smooth film was only 0.19, which was one-tenth of that obtained in water-lubricated conditions. This value was distinctly lower than the films with loop, whorl, and arch textures, which yielded values of 0.94, 0.75, and 1.33 in the same friction condition. The films with the arch patterns displayed lower COF values in dry and water-lubricated conditions. The arch patterned film demonstrated a higher COF value in oil-lubricated conditions than the other two fingerprint-like textures.

3.3 Tip pinch performance

The tip pinch tests were performed in dry, water-lubricated, and oil-lubricated conditions to imitate the daily use of human hands (Figs. 3(a) and 3(b)). The red dotted lines in Fig. 3(a) denote the position of the silicone rubber film. The left side of Fig. 3(c) shows the weight of the object grasped by the soft robotic hand when the film contacts the flat surface. After the

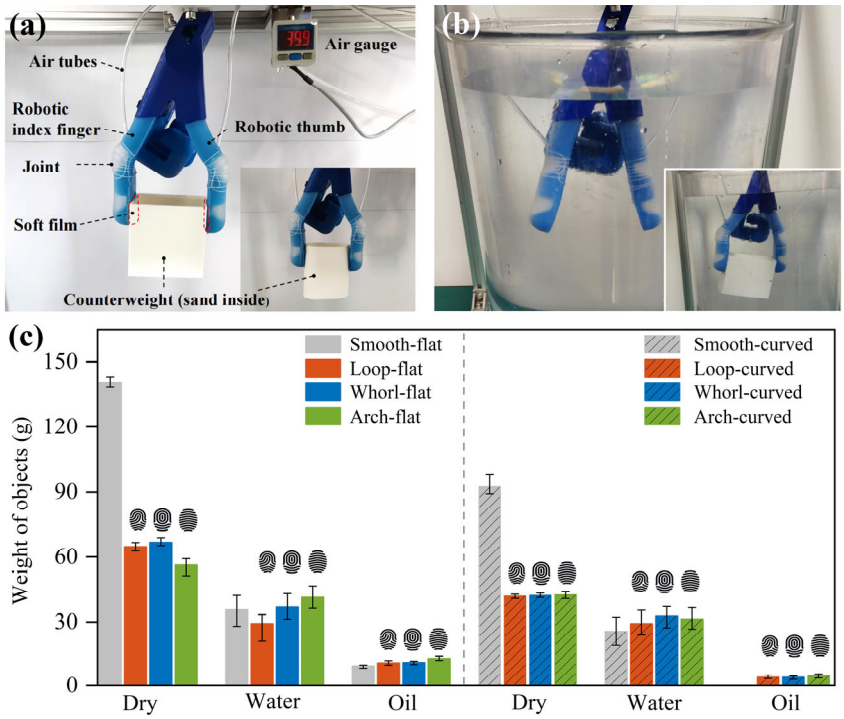

Fig. 3 (a) Tip pinch platform based on the soft robotic hand, (b) underwater tip pinch tests, and (c) weights of the objects with flat or curved surfaces that the soft hand can grasp.

smooth film was attached, the weight the soft hand could grip was significantly higher than that of the fingerprint-like films, reaching 140.47 g, which was consistent with the tribological test results. However, when immersed in water, the grasping weight of the smooth film was the same as that of the loop and arch films, at about 40 g. When oil was used as a lubrication medium, the grasping weights of the four films reduced significantly by about 10 g. The grasping ability of the fingerprint-like film was slightly better, with a weight reaching 12.80 g.

The right-hand side of Fig. 3(c) shows the weight of the object grasped by the soft robotic hand when the film contacts the curved surface. The soft hand could not grip the plastic box after adding the smooth film in oil-lubricated conditions, while the fingerprint-like film allowed the lubrication oil to pass through the fingerprint valleys, facilitating successful object grasping (3.93–4.5 g).

3.4 Impact of the surface texture on the tribological properties

Under dry friction conditions, a strip contact surface with a width of 2*a* was formed when the fingerprint peaks contacted the glass plate under a specific load (Fig. 4(a)). The same spacing between the fingerprint peaks and valleys can be equated to the same length of the fingerprint peaks in contact with a flat surface and the same contact area. While under lubricated conditions, the soft hand with fingerprint-like textures displayed a better grasping ability compared to the smooth surface. For the smooth surface, a lubricating film formed between the silicone rubber and the glass, separating the mating surfaces and restricting the actual contact area (Fig. 4(b)). As shown in Fig. 4(c), the grooves of the fingerprint-like textures allowed the lubrication medium to pass through, permitting the fingerprint peaks to directly contact the glass to increase the actual contact area. In addition, the grooved structure makes the tips deform easily, providing higher deformation force. Thus, the comprehensive frictional forces, which is composed of adhesion component and deformation component for elastic material, of fingerprint-like textures are higher than that of smooth surface.

According to the model consisting of an elastic cylinder in contact with a rigid plane, half the width of the contact surface a is expressed as [33]:

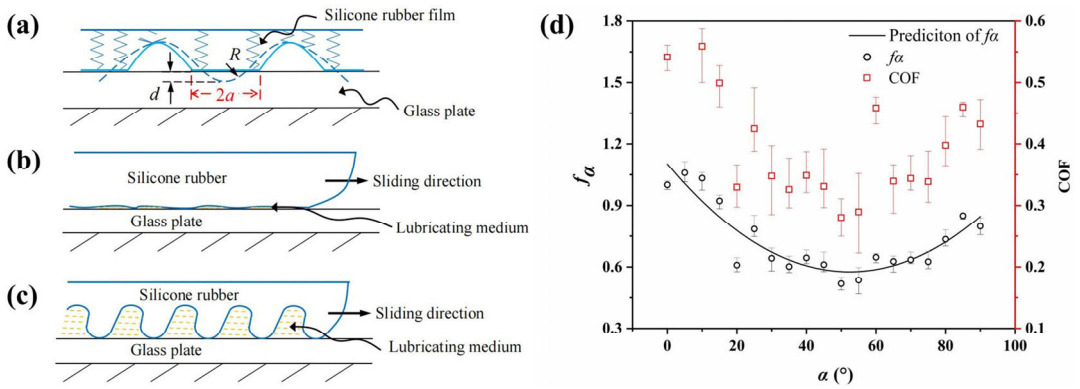

Fig. 4 (a) Schematic diagram of the contact deformation between the silicone rubber film and glass plate. (b, c) Schematic diagrams of the deformation of the silicone rubber with a smooth surface or fingerprint-like texture during the sliding process. (d) Experimental data and predicted curve of f_α and the corresponding COF.

$$a \approx \sqrt{2Rd} \tag{1}$$

where R is the cross-sectional radius of the fingerprint peak and d is the depth of the pressed silicone rubber.

As shown in Fig. 2, each fingerprint peak presented a relatively smooth ridge-like protrusion in the absence of contact. The 3D contact problem was mapped to a one-dimensional contact problem using the dimension reduction method [33]. According to the standard model of tribology, $F_s = \tau \cdot A$, τ was the interfacial shear strength, and A was the true contact area. Several fingerprint peaks were divided into n parts according to length, with i representing any of them, while $0 < i \le n$ and each segment was $\overrightarrow{l_{i,\alpha}}$.

$$F_s = \sum_{i=1}^{n} \tau \cdot A = \sum_{i=1}^{n} \tau \cdot 2a \cdot \overrightarrow{l_{i,a}} \tag{2}$$

where F_s is the sliding force, and l is the total length of the fingerprint peak. The sliding friction force of each fingerprint peak section relates to the contact angle, α, introducing the correction factor f_α related to α.

$$f_a = \left(\frac{\tau_a \cdot \left| \overrightarrow{l_{i,a}} \right|}{\tau_{a=0} \cdot \left| \overrightarrow{l_{i,a=0}} \right|} \right) \tag{3}$$

$$F_s = \sum_{i=1}^{n} \tau \cdot 2a \cdot \overrightarrow{l_{i,a}} \cdot f_a \tag{4}$$

The correction factor f_α was determined experiment ally. From the transverse stripe to the longitudinal stripe, α increased from 0° to 90°, while the equidistant transverse stripe silicone rubber film was prepared using 5° as the interval. The COF was measured using the previous tribological test platform, as shown in Fig. 4(d). The fitting correction factor f_α prediction curve was expressed as

$$f_\alpha = 1.1021 - 0.0200548 \cdot \alpha + 0.000191256 \cdot \alpha^2 \tag{5}$$

Image analysis was performed on the fingerprint-like patterns. The texture patterns in the image consisted of several pixel points, each of which presented a different color. Therefore, edge detection was performed on the line composed of blue pixels to obtain a binary edge image with white edge lines (Figs. S5(a) and S5(b) in the ESM). Then, line detection algorithms based on the Hough transform [34] were used to detect a continuous set of points, as shown in Fig. S5(c) in the ESM. The data of all the short line inclination angles were obtained with an interval of 1°, while the inclination angle proportions were calculated as shown in Fig. 5.

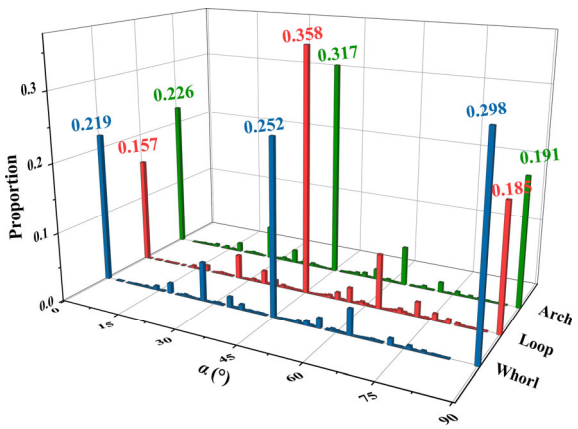

Fig. 5 Inclination angle proportion of the lines.

The inclination angle was divided into three intervals, namely the high-impact factor interval (HIFI), the medium-impact factor interval (MIFI), and the low-impact interval (LIFI), at 0°–30°, 31°–70°, and 71°–90°, respectively. A summary of the fingerprint-like pattern proportions in the intervals is shown in Table 1. The loop proportion in HIFI was small at only about 0.217, while the LIFI value was around 0.552, which was consistent with the lower COF of the loop pattern. Although the whorl and arch patterns displayed almost the same proportions in HIFI, the whorl proportion was relatively high in MIFI (0.319) and low in LIFI (0.368), which was consistent with the highest whorl COF.

Table 1 Inclination angle proportions of the lines in the intervals.

	HIFI 0° to 30°	MIFI 31° to 70°	LIFI 71° to 90°	Number of lines
Whorl	0.316279070	0.368168605	0.319476744	7,672
Loop	0.217216643	0.551936872	0.231850785	6,880
Arch	0.314781022	0.465589155	0.219629823	6,971

4 Conclusions

The tribological performance of silicone rubber films with a smooth surface and loop, whorl, and arch textures is evaluated to examine the effect of a fingerprint-like microstructure on the grasping ability of a soft hand. The coefficient of friction (COF) of the fingerprint-like textural films gradually stabilizes with higher relative sliding velocity/contact pressure while increasing significantly compared with the smooth surface in oil-lubricated conditions. The experimental results show that the COF depends to some extent on the texture pattern of the film. Although the arch-like film displays the lowest COF in dry conditions, it is substantially higher than the other films in oil-lubricated conditions. Similarly, in water- and oil-lubricated conditions, the grasping weight of the soft hand is markedly increased by the arch-like film during the tip pinch test.

The fingerprint-like films show different COF values and grasping firmness during the tribological and tip pinch tests. However, their numerical size relationships are not intuitive and stable enough. This can be attributed to the system errors of the test platform and complex environmental variables. The contact mechanics and tribological theoretical analysis indicate that the sliding friction force of each fingerprint peak is related to the inclination angle, α. Common transverse and longitudinal stripes account for the largest correction factor, increasing their sliding friction to a maximum. Obviously, fingerprint-like textures improves tip pinch performance in oil-lubricated conditions, which is attributed to higher actual contact area between the two surfaces and easily deformation of the grooved tips. The soft hand with the fingerprint-like textures displays better grasping ability compared to the smooth surface.

Our previous research focused on the tribological properties of a single contact on a smooth surface. However, most practical robotic grasping is considerably more complex. In actual hand and grasping scenarios, flat finger pads can often only align with the flat surfaces of flat grippers, especially parallel grippers. Most other hand object configurations that rely on multiple contacts result in multiple line or point contacts. Moreover, the force direction of the human finger pad in contact with the object is random relative to the fingerprint. Therefore, the high-impact factor interval (HIFI) position may be influenced by other areas in practice. Future research intends to collect and create enough irregular pattern samples to comprehensively examine their performance in all contact directions (360°) and obtain the optimal performance pattern via machine learning. And we hope to combine more work related to human touch, on the basis of understanding the ability of humans to grasp in favorable and unfavorable situations [35], to carry out the work of grasping by robotic hands.

Acknowledgements

This work is supported by the Science Foundation of China University of Petroleum-Beijing (Nos. 2462020XKJS01 and 2462020YXZZ046) and National Key R&D Program of China (No. 2017YFC0805800).

Electronic Supplementary Material: Supplementary material is available in the online version of this article at https://doi.org/10.1007/s40544-022-0688-4.

References

[1] Shintake J, Cacucciolo V, Floreano D, Shea H. Soft robotic grippers. *Adv Mater* **30**(29): 1707035 (2018)

[2] Langowski J K A, Sharma P, Shoushtari A L. In the soft grip of nature. *Sci Robot* **5**(49): eabd9120 (2020)

[3] Laschi C, Cianchetti M, Mazzolai B, Margheri L; Follador M, Dario P. Soft robot arm inspired by the octopus. *Adv Robot* **26**(7): 709–727 (2012).

[4] Martinez R V, Branch J L, Fish C R, Jin L H, Shepherd R F, Nunes R M D, Suo Z G, Whitesides G M, George M. Robotic tentacles with three-dimensional mobility based on flexible elastomers. *Adv Mater* **25**(2): 205–212 (2013)

[5] Tiefeng S, Mingyu D, Guanjun B, Bao G J, Yang Q H. Fruit harvesting continuum manipulator inspired by elephant trunk. *Int J Agr Biol Eng* **8**(1): 57–63 (2015)

[6] Xie Z, Domel A G, An N, et al. Octopus arm-inspired tapered soft actuators with suckers for improved grasping. *Soft Robot* **7**(5): 639–648 (2020)

[7] Galloway K C, Becker K P, Phillips B, Kirby J, Licht S, Tchernov D, Wood R J, Gruber D F. Soft robotic grippers for biological sampling on deep reefs. *Soft Robot* **3**(1): 23–33 (2016)

[8] Liao B, Zang H, Chen M, Wang Y, Lang X, Zhu N N, Yang Z, Yi Y. Soft rod-climbing robot inspired by winding locomotion of snake. *Soft Robot* **7**(4): 500–511 (2020)

[9] Deimel R, Brock O. A novel type of compliant and underactuated robotic hand for dexterous grasping. *Int J Robot Res* **35**(1–3): 161–185 (2016)

[10] Shahid Z, Glatman A L, Ryu S C. Design of a soft composite finger with adjustable joint stiffness. *Soft Robot* **6**(6): 722–732 (2019)

[11] Zhang H, Kumar A S, Chen F, Fuh J Y H, Wang M Y. Topology optimized multimaterial soft fingers for applications on grippers, rehabilitation, and artificial hands. *IEEE ASME T Mech* **24**(1): 120–131 (2019)

[12] Zhang N, Ge L, Xu H, Zhu X, Gu G. 3D printed, modularized rigid-flexible integrated soft finger actuators for anthropomorphic hands. *Sens Actuat A Phys* **312**(1): 112090 (2020)

[13] Wang W, Yu C Y, Abrego Serrano P A, Ahn S H. Shape memory alloy-based soft finger with changeable bending length using targeted variable stiffness. *Soft Robot* **7**(3): 283–291 (2020)

[14] Subramaniam V, Jain S, Agarwal J, Alvarado P V Y. Design and characterization of a hybrid soft gripper with active palm pose control. *Int J Robot Res* **39**(14): 1668–1685 (2020)

[15] Kim D, Yun D. A study on the effect of fingerprints in a wet system. *Sci Rep* **9**: 16554 (2019)

[16] Gechev A. Fluid containing structures in the tips of the fingers and toes delineated by ultrasound imaging before and after induced skin wrinkling. *Sci Rep* **9**: 1640 (2019)

[17] Davis N J. Water-immersion finger-wrinkling improves grip efficiency in handling wet objects. *PLoS One* **9**(2): 20120999 (2021)

[18] Trinh H X, Ho V A, Shibuya K. Theoretical foundation for design of friction-tunable soft finger with wrinkle's morphology. *IEEE Robot Autom Let* **4**(4): 4027–4034 (2019)

[19] Changizi M, Weber R, Kotecha R, Palazzo J. Are wet-induced wrinkled fingers primate rain treads. *Brain Behav Evolut* **77**(4): 286–290 (2011)

[20] Hao Y, Biswas S, Hawkes E W, Wang T M, Zhu M J, Wen L, Visell Y. A multimodal, enveloping soft gripper: Shape conformation, bioinspired adhesion, and expansion-driven suction. *IEEE T Robot* **37**(2): 350–362 (2021)

[21] Seibel A, Yildiz M, Zorlubas A B. A gecko-inspired soft passive gripper. *Biomimetics* **5**(2): 1–12 (2020)

[22] Wang H, Xu H, Abu-Dakka F J, Kyrki V, Yang C, Li X, Chen S. A bidirectional soft biomimetic hand driven by water hydraulic for dexterous underwater grasping. *IEEE Robot Autom Let* **7**(2): 2186–2193 (2022)

[23] Wang H, Abu-Dakka F J, Le T N, Kyrki, V, He X. A novel design of soft robotic hand with a human-inspired soft palm for dexterous grasping. *arXiv* 2009.00979 (2020)

[24] Hussain I, Al-Ketan O, Renda F, Malvezzi M, Prattichizzo D, Seneviratne L, Abu Al-Rub R K, Gan D M. Design and prototyping soft–rigid tendon-driven modular grippers using interpenetrating phase composites materials. *Int J Robot Res* **39**(14): 1635–1646 (2020)

[25] Pozzi M, Marullo S, Salvietti G, Bimbo J, Malvezzi M, Prattichizzo D. Hand closure model for planning top grasps with soft robotic hands. *Int J Robot Res* **39**(14): 1706–1723 (2020)

[26] Teeple C B, Koutros T N, Graule M A, Wood R J. Multi-segment soft robotic fingers enable robust precision grasping. *Int J Robot Res* **39**(14): 1647–1667 (2020)
[27] Mannam P, Rudich A, Zhang K, Veloso M, Kroemer O, Temel F Z. A low-cost compliant gripper using cooperative mini-delta robots for dexterous manipulation. In *Robotics: Science and Systems XVII, Held Virtually*. 2021.
[28] Abondance S, Teeple C B, Wood R J. A dexterous soft robotic hand for delicate in-hand manipulation. *IEEE Robot Autom Let* **5**(4): 5502–5509 (2020)
[29] Sinatra N R, Teeple C B, Vogt D M, Parker K K, Gruber D F, Wood R J. Ultragentle manipulation of delicate structures using a soft robotic gripper. *Sci Robot* **4**(33): eaax5425 (2019)
[30] Rus D, Tolley M T. Design, fabrication and control of soft robots. *Nature* **521**: 467–475 (2015)
[31] Hao T, Xiao H, Liu S, Zhang C, Ma H. Multijointed pneumatic soft hand with flexible thenar. *Soft Robot* **9**(4): 745–753 (2022)
[32] Mathiowetz V, Kashman N, Volland G, Weber K, Dowe M, Rogers S. Grip and pinch strength: normative data for adults. *Arch Phys Med Rehab* **66**(2): 69–74 (1985)
[33] Valentin L P, Markus H. *Method of dimensionality reduction in contact mechanics and friction*. Berlin (Germany): Springer, 2015.
[34] Yuan H, Ma H. Line detection for point set of varying discrete degrees. In *Fourth International Conference on Image and Graphics (ICIG 2007)*, Sanya, China, 2007: 453–458.
[35] Tomlinson, S P, Davis, N J, Morgan, H M, Bracewell R M. Hemispheric specialisation in haptic processing. *Neuropsychologia* **49**(9): 2703–2710 (2011)

Tianze HAO. He received her bachelor degree in mechanical engineering and automation in 2018 from Northeast Petroleum University, China. After then, he was a Ph.D. student in mechanical engineering in China University of Petroleum-Beijing, China. His research interests include soft robotic and surface engineering.

Huaping XIAO. He received his bachelor degree in 2006 from Tianjin University, Tianjin, China and master degree in 2011 from Tsinghua University, Beijing, China. He has earned Ph.D. degree in mechanical engineering in 2014 from Texas A&M University (TAMU), USA. He joined the College of Mechanical and Transportation Engineering at China University of Petroleum from 2014. His current position is an associate professor. His research areas include tribology properties and wear behaviors under complicated work condition and bio-related tribological systems.

Shuhai LIU. He received his Ph.D. degree in mechanical engineering in 2009 from Tsinghua University, Beijing, China. He joined the College of Mechanical and Transportation Engineering at China University of Petroleum-Beijing from 2009. His current position is a professor and the assistant dean of the college. His research interests include tribology, surface science, and petroleum science.

Yibo LIU. He received his bachelor degree in mechanical engineering and automation in 2018 from China University of Petroleum-Beijing, China. After then, He was a Ph.D. student in mechanical engineering at the same university. His research interests include soft robotic and surface engineering.